Compressively Sensed Ultrasound Radio-frequency Data Reconstruction Using the Combined Curvelets and Wave Atoms Basis

Mohammad Arafat Hussain
Department of EEE, Eastern University
Dhaka–1205, Bangladesh
Email: arafat.eee@easternuni.edu.bd

Riad Mashrub Shourov
Directorate of Technical Education
Dhaka–1207, Bangladesh
Email: riadmashrub.shourov@gmail.com

***Abstract*—In this paper, we propose a novel data reconstruction method for the compressively sensed ultrasound radio-frequency (RF) data using the combined curvelets- and wave atoms- (CCW) based orthonormal basis. Typically, the curvelets-based reconstruction better preserves the image features while the wave atoms-based reconstruction better preserves the oscillatory patterns of the typical ultrasound RF signals. We exploit the advantages from both the sparsifying bases via concatenating them where the RF reconstruction is done from the larger coefficients of the combined basis. We show that the CCW-based reconstruction method better recovers the RF oscillatory patterns as well as preserves the image features better than those of the curvelets- and wave atoms-based reconstruction methods alone. We find improvement with respect to the current methods of approximately 58% and 64% in terms of the normalized mean square error for the reconstructed synthetic phantom and *in vivo* RF data, respectively. We also show visual performance improvement in the B-mode images of approximately 33% and 44% in terms of the mean structural similarity for the synthetic phantom and *in vivo* data, respectively.**

***Keywords*—Ultrasound, curvelets, wave atoms, compressive sensing, sparsity.**

I. Introduction

Ultrasound (US) imaging has become an essential part of clinical routine that produces real-time images of patient anatomy. As a non-ionizing and low-cost modality, US has a number of advantages over other medical imaging modalities like non-invasiveness, portability, and versatility. However, handling a large amount of US data during real-time imaging as well as its transmission at low bit rate (and without any perceived loss of image quality) in tele-medicine are considered limiting factors [1].

The recently introduced compressive sensing (CS) theory allows to recover a signal sampled below the Nyquist sampling limit [2] under certain assumptions. CS provide optimized ultrasound imaging solutions that also has the potential to offer a coherent framework for image analysis, object detection, and information extraction [4]. CS can also improve efficiency of triplex acquisitions for CFM/B-mode/Doppler or 3D imaging using matrix arrays [4]. So far, a number of sparsifying bases for the reconstruction of compressively sensed US have been proposed in literature like the Fourier [1], wavelets [2] , wave atoms [2], [3], curvelets [3], and Bayesian [4], [5] bases. The Bayesian framework-based methods [4], [5] have a limitation that the data are projected on a random Gaussian basis prior to the reconstruction which is difficult to apply in practice [2]. Recently, the wave atoms-based reconstruction is shown better than those of the Fourier and wavelets bases [2] since it better reconstruct the oscillatory pattern of the ultrasound RF data. However, the major limitation of the wave atoms-based method is that it distorts the image features (e.g., lesion-soft tissue interfaces). On the other hand, the curvelets-based reconstruction [3] better preserves image features but produces noisy RF data which results in the distorted speckle patterns in the corresponding B-mode image.

In this paper, we propose a novel reconstruction method for the compressively sensed ultrasound RF data using the combined curvelets- and wave atoms-based orthonormal basis. We exploit the merits of both the sparsifying orthonormal bases via concatenating them where RF data is reconstructed from the larger coefficients of the combined basis. We use a synthetic phantom and *in vivo* patient data to validate the proposed method where we observe marked improvement in the normalized mean square error (NMSE) estimated from the reconstructed RF and B-mode data. We also observe considerable visual performance improvement in terms of the mean structural similarity (MSSIM) in the B-mode images estimated from the reconstructed RF data.

II. Methods

Our method is divided into two parts. In Sect. II-A, we discuss the restriction operator that is used to compressively sense the US RF data. Then, in Sect. II-B, we discuss the reconstruction of the RF signals from the sparse data using the combined curvelets and wave atoms.

A. Restriction Operator

2-dimensional (2D) CCW-based reconstruction is a sparse optimization problem. Although we discuss the CCW-based 2D data reconstruction procedure in this section but it is relatively straightforward to generalize the process to 3D. We define vec as a vectorization operator of a 2D data matrix and the reconstruction from a sparse 2D RF data follows the forward model as

$$\mathbf{b} = \mathbf{R}vec(F), \tag{1}$$

where $\mathbf{b} \in \mathbb{R}^N$ is the vector of acquired subsampled (sparse) 2D data with missing traces, $F \in \mathbb{R}^{N_a \times N_l}$ is the to-be-recovered 2D signal on a regular un-aliased output grid, N is

978-1-4673-7819-2/15/$31.00©2015 IEEE

the total number of samples in the subsampled RF data, and N_a and N_l are the total number of actual samples along each axial (i.e., scan-line) and lateral line of the RF data, respectively. In addition, $\mathbf{R} \in \mathbb{B}^{N \times N_a N_l}$ with $\mathbb{B} = \{0, 1\}$, is the restriction operator that collects N samples from the full RF data F and $N_a N_l \gg N$. Thus, $\mathbf{R}$ is a binary sampling matrix, and both the acquired data $\mathbf{b}$ and to-be-recovered data F depend on it.

B. CCW-based Reconstruction Method

The primary target of the CCW-based reconstruction method is to recover the original signal F as in Eqn. (1) using a combined orthonormal sparsifying domain that consists of curvelets and wave atoms coefficients. This equation is an under-determined inverse problem. The solution of this equation would be the model that agrees with incomplete data $\mathbf{b}$ after being restricted by restriction operator $\mathbf{R}$. We reformulate the problem in Eqn. (1) according to the compressive sampling theory as

$$\mathbf{b} = \mathbf{A}x \qquad \text{with} \qquad \mathbf{A} = \mathbf{R}\mathbf{S}^H, \tag{2}$$

where $\mathbf{S} = C \| W$ is the sparsifying transform that catenates two different sparsifying bases namely curvelets C and wave atoms W, $\|$ sign denotes catenation operator, $\mathbf{S}^H = C^H \| W^H$), and $x \in \mathbb{R}^P$ with $P > N$ is the redundant representation of the RF data in the sparsifying domain.

Finally, for randomized subsampling, Eqn. (2) can be written as [6]

$$\mathbf{A}^H(\mathbf{b}) = \mathbf{A}^H \mathbf{A} x \approx x + n, \tag{3}$$

where n represent the approximated additive white Gaussian noise due to the spectral leakage. The curvelets and wave atoms transforms give a compressible representation of $\mathbf{s}$ where $\mathbf{s}$ is the number of non-zero element in the sparsifying domain and therefore called $\mathbf{s}$-sparse. It is shown in [7] that for a matrix $\mathbf{A}$ with a specified isometry constant of the so-called restricted isometry property, optimization problem in Eqn. (2) can be solved as

$$\mathbf{P}: \begin{cases} \tilde{x} = \arg\min_x \| x \|_1 & \text{s.t.} \quad \mathbf{R}\mathbf{S}^H x = \mathbf{b}, \\ \tilde{F} = \mathbf{S}^H \tilde{x}, \end{cases} \tag{4}$$

where $\| x \|_1 = \sum_{i=1}^{P} \mid x_i \mid$ is the l_1 norm. The recovered vector that solves $\mathbf{P}$ is $\tilde{x}$, and $\tilde{F}$ is the estimate of the recovered RF data.

III. Validation Setup

1) Synthetic Phantom: We built a 40mm×40mm×5mm synthetic phantom using the ultrasound simulation software Field II [8]. Our phantom corresponds to a cyst phantom containing a total of 50,000 point scatterers. An ultrasonic transducer of center frequency, f_0 = 5MHz, sampling frequency, f_s = 20MHz, and band-width = 50% was used to simulate the phantom scan from the top. The total number of scan lines was set to 128. The phantom contained three hyper echoic inclusions of diameters 5mm, 4mm and 3mm from top to bottom, as well as three hypo echoic inclusions of diameters 3mm, 4mm and 5mm from top to bottom. The hypo echoic inclusions contained no scatterers. However, in the background and hyper echoic inclusions, the spatial distribution of the scatterers was uniform. The scattering amplitude followed a zero mean Gaussian distribution. The amplitude of the scatterers' inside the hyper echoic inclusions was set to ten times of that of the background.

2) Real In Vivo Data: We use three sets of *in vivo* US data from patients undergoing open surgical RF thermal ablation for primary or secondary liver cancer and proper prior consent was obtained [9]. US data were acquired using a RITA Model 1500 XRF generator (Rita Medical Systems, Fremont, CA) at a transducer center frequency, f_0 = 7.27MHz and sampling frequency, f_s = 40MHz. The study was approved by an institutional review board.

IV. Results and Discussion

We provide comparative results of our proposed method with the wave atoms- [2], [3] and curvelets-based [3] RF signal reconstruction methods. In addition to the evaluation by visual inspection, we compare the performances of these methods in terms of NMSE and MSSIM [10]. The quality metric NMSE is defined as

$$\text{NMSE} = \frac{1}{N_a \times N_l} \sum_{m=1}^{N_a} \sum_{n=1}^{N_l} [F(m,n) - \tilde{F}(m,n)]^2. \tag{5}$$

For the B-mode images, we replace F and $\tilde{F}$ in Eqn. (5) with their corresponding B-mode images B and $\tilde{B}$, respectively. Note that we normalize F, $\tilde{F}$, B, and $\tilde{B}$ before estimating the NMSE. Typically, it is assumed that the human visual perception is highly adapted for extracting structural information from a scene. The MSSIM is shown to be an excellent predictor of the image perceptual quality. It considers contrast, luminance and structural similarity between the B and $\tilde{B}$ to compute the value of the index. So, as closer the MSSIM index to the unity is, more visually closer the B and $\tilde{B}$ are. Due to space limitation, we do not provide the detail description of the MSSIM estimation process in this paper. Also note that the 'percentage (%) of data removed' we denote in this paper is estimated with respect to the original sampling rate of a particular data.

A. Synthetic Phantom Results

To illustrate the efficacy of our proposed method in preserving the important pathological information in the reconstructed data than those by the individual curvelets- and wave atoms-based methods, we show the corresponding B-mode images of the synthetic data in Figs. 1(b)–(d). We see that the curvelets-based reconstruction method well preserves the inclusion boundaries but the speckle pattern in the soft tissue region looks noisy compared to the actual image (see Figs. 1(a) and (b)). On the other hand, the wave atoms-based method produces better speckle pattern but distorts the inclusion boundaries (shown with white arrows in Fig. 1(c)). In contrast, the proposed CCW-based method well preserves the inclusion boundaries as well as produces better speckle patterns in the soft tissue region as seen in the B-mode image (see Fig. 1(d)).

We also demonstrate the quantitative performance comparisons of the curvelets-, wave atoms-, and CCW-based methods in terms of NMSE and MSSIM metrics in Figs. 1(e)-(g). In Figs. 1(e) and (f), we plot the estimated NMSE between the actual and reconstructed RF data, and between the actual and reconstructed B-mode data, respectively, at

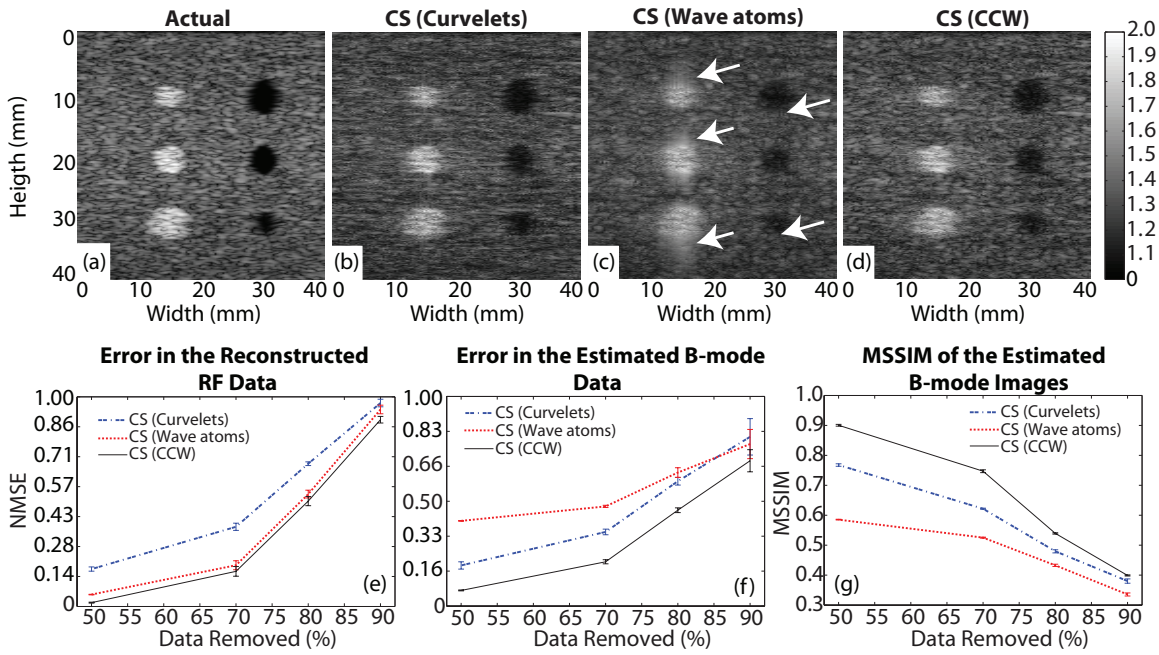

Fig. 1. Illustration of the RF data reconstruction performances of different methods using the synthetic phantom. (a) Actual B-mode image. Estimated B-mode images from the RF data reconstructed by (b) curvelets-based, (c) wave atoms-based, and (d) CCW-based methods for 80% subsampling. (e) NMSE of the reconstructed RF data, (f) NMSE of the estimated B-mode images from the reconstructed RF data, and (g) MSSIM of the estimated B-mode images from the reconstructed RF data.

different subsampling rates. Here we see that the curvelets-based method performs the worst in RF reconstruction (see Fig. 1(e)) although it better preserves the inclusion boundaries than the wave atoms-based method (see Fig. 1(f)) which supports our claims during visual inspection. However, the proposed reconstruction method outperforms both the methods in RF reconstruction and image feature preservation at all the subsampling rates as depicted in Figs. 1(e) and (f). In addition, since the proposed reconstruction method produces the best RF data, the resulting B-mode image matches the actual B-mode image best at all the subsampling rates than those of the curvelets- and wave atoms-based reconstruction methods as evident from the MSSIM plots in Fig. 1(f).

B. In Vivo Results

We show the qualitative performance comparison of the RF reconstruction as well as the image feature preservation by the curvelets-, wave atoms- and CCW-based methods using the *in vivo* data in Fig. 2. In Figs. 2(a)–(c), we see that the wave atoms-based reconstruction results distorted lesion boundaries/features in the B-mode images (see red arrows in Figs. 2(a)-(c)). On the other hand, the curvelets-based reconstruction method well preserves the lesion boundaries/features but the speckle pattern in the soft tissue region looks noisy compared to the actual image. In contrast, similar to the synthetic data, the proposed CCW-based method well preserves the image features as well as produces better speckle patterns in the soft tissue region as seen in the corresponding B-mode images (see Figs. 2(a)-(c)).

We also illustrate the quantitative performance comparisons of the curvelets-, wave atoms-, and CCW-based methods in terms of NMSE and MSSIM metrics using the *in vivo* data in Figs. 2(d)-(l). In Figs. 2(d)–(f), we see that the mean NMSE values for the reconstructed RF data by the curvelets-based method are the highest while by the CCW-based method are the lowest in all the patient cases at all subsampling rates. Also in case of the B-mode images as shown in Figs. 2(g)–(i), the mean NMSE values by the CCW-based method are the lowest in all the patient cases at all subsampling rates. However, by the increase of the data removal percentage, the performance of the wave atoms-based method becomes better than that of the curvelets-based method for B-mode images. We also quantitatively compare the visual performance of the curvelets-, wave atoms-, and CCW-based methods in terms of MSSIM in Figs. 2(j)–(l). We see from these figures that the mean MSSIM indexes of the proposed method are the highest in all the patient cases at all subsampling rates. In contrast, the mean MSSIM indexes of the wave atoms-based method are the lowest in all the patient cases at all subsampling rates.

V. Conclusions

In this paper, we developed a novel data reconstruction method for the compressively sensed ultrasound RF data using the combined curvelets- and wave atoms-based orthonormal basis. As the curvelets-based reconstruction better preserves the image features while the wave atoms-based reconstruction better preserves the oscillatory patterns of the typical ultrasound RF signals, we exploited the advantages from both the sparsifying orthonormal bases via concatenating them where optimized sparse representation is obtained from the larger coefficients of the combined basis. We shown that the CCW-based reconstruction method better recovers the typical RF oscillatory pattern as well as preserves the image feature better than those of the curvelets- and wave atoms-based reconstruction method alone. We demonstrated our improved performance with respect to the current methods for a wide range of validation data including a simulated synthetic phantom and

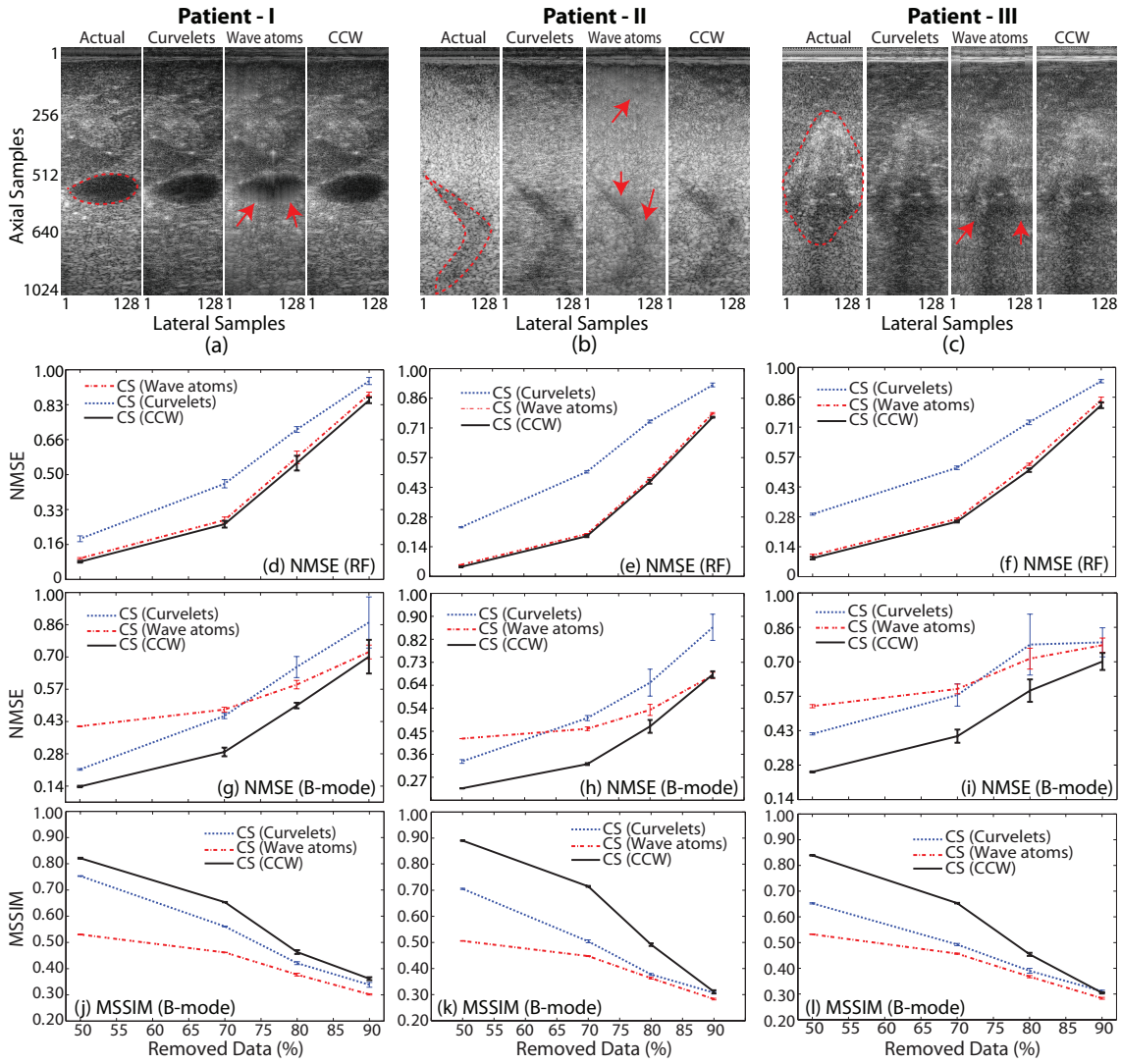

Fig. 2. Illustration of the RF data reconstruction performance of different methods using 3 sets of *in vivo* data. (a)-(c) Actual and estimated B-mode images from the reconstructed RF data (80% subsampled), (d)-(f) NMSE of the reconstructed RF data, (g)-(i) NMSE of the estimated B-mode images from the reconstructed RF data, and (j)-(l) MSSIM of the estimated B-mode images from the reconstructed RF data.

in vivo data. Our method demonstrated an improvement of approximately 58%, 80% and 33% on an average in the RF NMSE, B-mode NMSE and B-mode MSSIM, respectively, in the synthetic data test. Our method also shown an improvement of approximately 64%, 50% and 44% on an average in the RF NMSE, B-mode NMSE and B-mode MSSIM, respectively, in the *in vivo* data test.

REFERENCES

[1] C. Quinsac, A. Basarab, J.-M. Girault, and D. Kouamé, "Compressed Sensing of Ultrasound Images: Sampling of Spatial and Frequency Domains," In: *IEEE Workshop on Signal Processing Systems (SIPS)*, pp. 231–236, 2010.

[2] H. Liebgott, R. Prost, and D. Friboulet,"Pre-beamformed RF Signal Reconstruction in Medical Ultrasound Using Compressive Sensing," *Ultrasonics*, vol. 53, pp. 525–533, 2013.

[3] M. F. Schiffner, T. Jansen, and G. Schmitz, "Compressed Sensing for Fast Image Acquisition in Pulse-Echo Ultrasound," *Biomedical Engineering*, vol. 57, no. 1, pp. 192–195, 2012.

[4] A. Achim, B. Buxton, G. Tzagkarakis, and P. Tsakalides,"Compressive Sensing for Ultrasound RF Echoes Using α-Stable Distributions," In: *IEEE Annual International Conference of Engineering in Medicine and Biology Society (EMBC)*, pp. 4304–4307, 2010.

[5] A. Achim, A. Basarab, G. Tzagkarakis, P. Tsakalides, and D. Kouamé, "Reconstruction of Compressively Sampled Ultrasound Images Using Dual Prior Information," In: *2014 IEEE International Conference on Image Processing (ICIP)*, pp. 1283–1286, 2014.

[6] G. Hennenfent and F. J. Herrmann, "Simply Denoise: Wavefield Reconstruction Via Jittered Undersampling,"*Geophysics*, vol. 73, no. 3, pp. V19–V28, 2008.

[7] E. J. Candes, J. Romberg, and T. Tao, "Robust Uncertainty Principles: Exact Signal Reconstruction From Highly Incomplete Frequency Information," *IEEE Transactions on Information Theory*, vol. 52, no. 2, pp. 489–509, 2006.

[8] J. A. Jensen, "Field: A Program for Simulating Ultrasound Systems," In: *10th Nordicbaltic Conf. on Biomed. Imag.*, vol. 4, pp. 351–353, 1996.

[9] H. Rivaz, E. M. Boctor, M. A. Choti, and G. D. Hager, "Real-time Regularized Ultrasound Elastography," *IEEE Trans. Med. Imag.*, vol. 30, no. 4, pp. 928–945, 2011.

[10] Z. Wang, A. C. Bovik, H. R. Sheikh, and E. P. Simoncelli, "Image Quality Assessment: From Error Visibility to Structural Similarity," *IEEE Trans. Image Process.*, vol. 13, no. 4, pp. 600–612, 2004.